Conductive mechanism in memristor at the thinnest limit: The case based on monolayer boron nitride

Xiao-Dong Li, iD Nian-Ke Chen, Bai-Qian Wang, et al.

View Online   Export Citation   CrossMark

ARTICLES YOU MAY BE INTERESTED IN

Conductive mechanism in memristor at the thinnest limit: The case based on monolayer boron nitride

Xiao-Dong Li, Nian-Ke Chen,[a] 🔲 Bai-Qian Wang, and Xian-Bin Li[a] 🔲

AFFILIATIONS

State Key Laboratory of Integrated Optoelectronics, College of Electronic Science and Engineering, Jilin University,
130012 Changchun, China

[a]Authors to whom correspondence should be addressed: chennianke@jlu.edu.cn and lixianbin@jlu.edu.cn

ABSTRACT

Atomic picture and electronic transport property are taken into account to investigate the nonvolatile resistive switching mechanism of a memristor at the thinnest limit, just based on one monolayer hexagonal boron nitride (h-BN). It is demonstrated that the intrinsic van der Waals gaps between electrodes and monolayer h-BN ensure the high resistance state (HRS). However, the absorption/desorption of a metallic-electrode atom on the one side of the h-BN can hardly switch the device to hold the experimentally observed ON/OFF current ratio. It is proposed that the electrode atom should penetrate the h-BN sheet via boron vacancy (V_B) to form a full conductive atomic filament for an effective low resistance state. The current signal of this V_B pinning Au conductive filament can reach up to three orders of magnitude higher than that of the HRS. The energy barrier for one Au atom to pass through V_B is also reasonably as low as 0.832 eV. Molecular dynamics simulation further manifests the nonvolatility of this atomic conductive filament at the limit that could even maintain stability at 500 K. This work offers a key working picture in memristors at their thinnest limit, which provides a valuable reference to the development of emerging memory/computing devices at the ultrathin scale.

With the rapid development of the data-intensive industry, such as machine learning, Internet of Things, and piloted driving in recent years, high-performance computing and memory hardware are consequently required.[1–3] The in-memory computing technology which can realize data processing and storage in the same physical unit,[4] has become a promising strategy to meet the demands.[5] For implementation of this technology, many kinds of nonvolatile memory[6–16] with excellent performance are developed to realize the co-location of logic and memory.[17] Among these devices, resistive random-access memory (RRAM), also called a memristor, has recently emerged as a promising candidate owing to its high-density storage, speed-sensitive switch, low power consumption, and simple device architecture.[18]

Two-dimensional RRAM devices, which inherit the excellent properties of 2D materials and have attracted widespread attention, are expected to have smaller sizes and higher integration density.[19,20] Moreover, the weak van der Waals (vdW) interaction of 2D heterojunctions can provide more degrees of freedom for lattice matching between electrodes and layered materials. Although nonvolatile

resistive switching (NVRS) behavior has been realized in a series of multilayer 2D materials,[21–30] the monolayer 2D materials were expected to have no NVRS phenomenon in a vertical metal–insulator–metal (MIM) configuration over a period of time owing to the difficulties in maintaining insulation.[31] However, most recently, Akinwande et al. demonstrated the NVRS effects in monolayer TMDs and even monolayer h-BN sandwiched between two metal electrodes in the vertical direction.[31–35] Then, Nikam et al. also found the similar NVRS behavior in monolayer h-BN.[36] The memristor based on ultrathin monolayer materials extends the scaling limit and provides opportunities for high-performance devices.

Unlike multilayer 2D-material-based RRAMs, which can form conductive filaments through grain boundaries,[27,29,37] the physical picture of a conductive channel in a single-layer 2D material based memristor is still under strong debate. It has been reported that the NVRS mechanism in these atomically thin memristors is dominated by the adsorption and desorption process of metal atoms in atomic sheets.[35,38] However, the density of states suggests that a very high defect concentration (as much as 25%) is needed to realize the large enough ON/OFF

ratio in the monolayer h-BN based memristor,[31] which is hard to adequately explain the NVRS phenomenon in these devices.

In this Letter, we investigate the conductive mechanism of the thinnest memristor based on monolayer h-BN vertically sandwiched between Au electrodes via density functional theory (DFT)[39,40] simulations combined with Keldysh nonequilibrium Green's function (NEGF) transport method.[41] It was found that the vdW gaps between electrodes and monolayer h-BN lead to an insulation characteristic in the vertical direction and, hence, ensure the high resistance state (HRS). When Au atoms penetrate the atomic sheet via boron vacancy (V_B), the full conductive filaments are formed, and thus, a low resistance state (LRS) is achieved. The current signal of this V_B pinning Au conductive filament can reach up to three orders of magnitude higher than that of the HRS, which is consistent with the experimental 10^3 ON/OFF ratio.[31,35] The energy barrier for Au atoms to pass through V_B is just 0.832 eV. The molecular dynamics simulation further demonstrates the nonvolatility of this atomically conductive filament could even maintain stability at 500 K. Our results provide a key picture of the resistive-switching mechanism in memristors at the thinnest limit, which provides valuable references to develop advanced memristors at the ultra-miniaturized scale.

DFT calculations were completed with the Vienna *ab initio* simulation package (VASP).[42] A nudged elastic band (NEB) method[43] was performed to study the energy barriers for Au atoms passing through the h-BN atomic sheet. The Perdew, Burke, and Ernzerhof (PBE) exchange–correlation functional within the generalized gradient approximation (GGA) was adopted here.[44] The 8×8 supercell of the monolayer h-BN sheet with a 15 Å vacuum layer is constructed to study the defect-and-adsorption-related structures and properties. The cutoff energy for plane wave expansion was 545 eV, and the Monkhorst–Pack k-point mesh grids of $1 \times 1 \times 1$, $3 \times 3 \times 1$, and $5 \times 5 \times 1$ were used for molecular dynamic (MD) simulation, structure relaxation, and density of states calculations, respectively. The convergence criterion for electronic self-consistent calculation was 10^{-6} eV.

The residual forces for structure relaxation and NEB calculations are less than 0.01 and 0.05 eV Å^{-1}, respectively. The MD simulations are run with a canonical ensemble (NVT) and a time step of 2.0 fs.

A supercell of 8×8 monolayer h-BN [sandwiched between two 7×7 Au (111) layers] is built. The MIM structures of Au-h-BN-Au are relaxed by VASP code. DFT-D3 correction is adopted to describe the vdW interactions. To reduce the tremendous computational cost, Au atom chains instead of Au (111) layers are used as electrodes (see Fig. S1 in the supplementary material for simplified models) to calculate I–V curves. Keldysh nonequilibrium Green's function and density functional theory (NEGF-DFT) quantum transport package Nanodcal[45] is employed to compute the I–V curves. Double-zeta polarized atomic orbital basis is used.[46] Atomic cores are defined by standard norm-conserving pseudopotentials with the local density approximation (LDA) exchange-correlation functional,[47] and $100 \times 100 \times 1$ k-points are chosen. The electronic temperature was set to 100 K. The cutoff of the real-space mesh was 80 Hartree.

Figure 1(a) shows a schematic of the memristor based on monolayer h-BN sandwiched between Au electrodes, which has been demonstrated as the thinnest nonvolatile memory.[31,35] The previous study regarded that Au atoms can be dissociated from electrodes and then adsorbed on just one side of monolayer h-BN under an electric field.[35] The adsorption of Au atoms may change the electronic density of states (DOS) of monolayer h-BN and, hence, is the key point to investigate the resistive switching mechanism.[31] To systematically estimate the influence of adsorptions, we investigate the structures and adsorption energies of Au atoms in different sites/defects of monolayer h-BN. The adsorption energy (E_a) is calculated using the following formula:

$$E_a = E_{Au+hBN} - E_{Au} - E_{hBN},$$

where E_{Au+hBN} is the total energy of Au adsorbed pristine or defective h-BN, E_{hBN} is the energy of pristine or defective h-BN, and E_{Au} is the energy of an isolated Au atom. Figures 1(b)–1(e) exhibit different adsorbed positions on pristine monolayer h-BN. It is clear that the Au
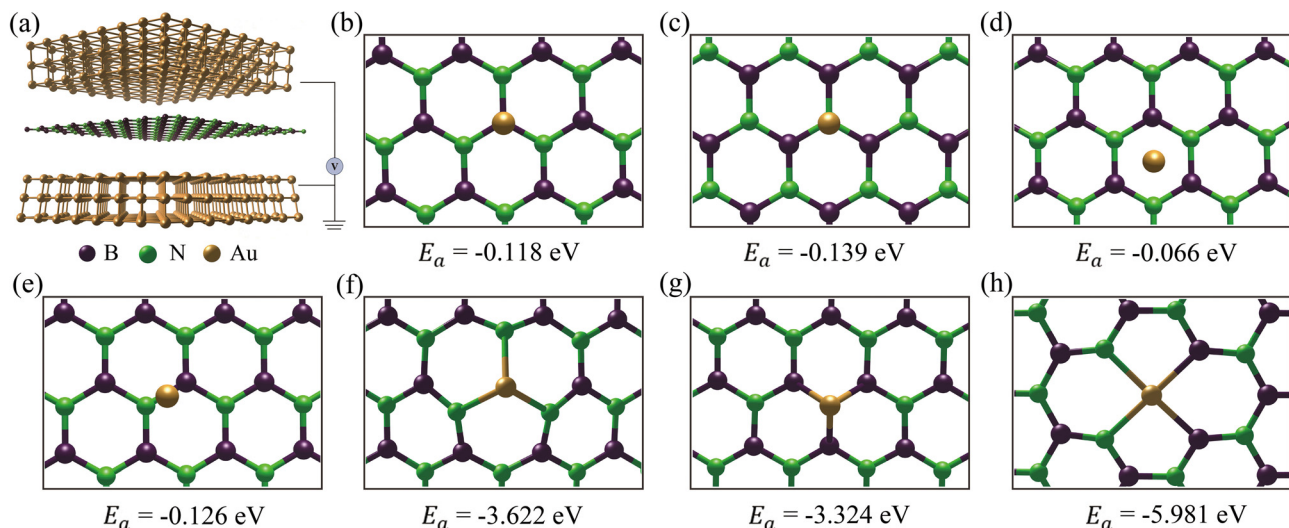
FIG. 1. (a) Schematic of a memristor based on one monolayer h-BN sandwiched between Au electrodes. (b)–(e) Adsorption of Au atoms on different sites of pristine monolayer h-BN, including: on the top of (b) boron atom, (c) nitrogen atom, (d) honeycomb, and (e) bridge site. (f)-(h) Adsorbed states of Au atoms on h-BN with (f) V_B, (g) V_N, and (h) V_{BN}.

atom is just physisorbed on pristine h-BN, because the adsorption energy is as low as $-0.066 \sim -0.139$ eV. This indicates the perfect h-BN hardly provides active sites to form stable conductive filaments. In contrast, the adsorptions of the Au atom on V_B, nitrogen vacancy (V_N), and divacancy (V_{BN}) are more stable with the energy of $-3.324 \sim -5.981$ eV, see Figs. 1(f)–1(h). Side views of these structures are presented in Fig. S2. It reflects the Au atom is chemisorbed on defective h-BN stably, which is consistent with the previous report.[48] In view of fact that multi-vacancy defects may result in Au-atom accumulation and easily lead to a short-circuit effect in devices (see the discussion later), we mainly focus on monovacancy defects.

To comprehend the conductive switching mechanism in the thinnest memristor, the NEGF-DFT method was used to simulate its $I–V$ characteristics. Figure 2(a) shows the schematic of the MIM structure in the calculations. The $I–V$ results in Fig. 2(b) manifest the monolayer h-BN with V_B could maintain a very good insulation as the

pristine h-BN does. However, the monolayer h-BN with V_N shows a significantly large leakage current, indicating a failure of offering a HRS for the memristor. The reason for this phenomenon will be discussed later. Considering the as-fabricated device is initially at the HRS,[31] we focus on V_B defects in the following studies. In fact, according to previous experimental reports,[49,50] V_B is indeed observed in h-BN.

Next, we try to understand possible factors that govern the conductance of this atomically thin memristor. According to previous reports,[51–53] the vdW gaps between electrodes and h-BN monolayer will set a barrier for vertical electronic emission. This should be the reason for maintaining insulation for the monolayer h-BN based memristor. In fact, the tunneling barrier induced by the vdW gap should be closely related to the vacuum level (E_0) and the Fermi level (E_F). To illuminate the current characteristics in the switching process, electronic DOS of a monolayer h-BN with different defects was
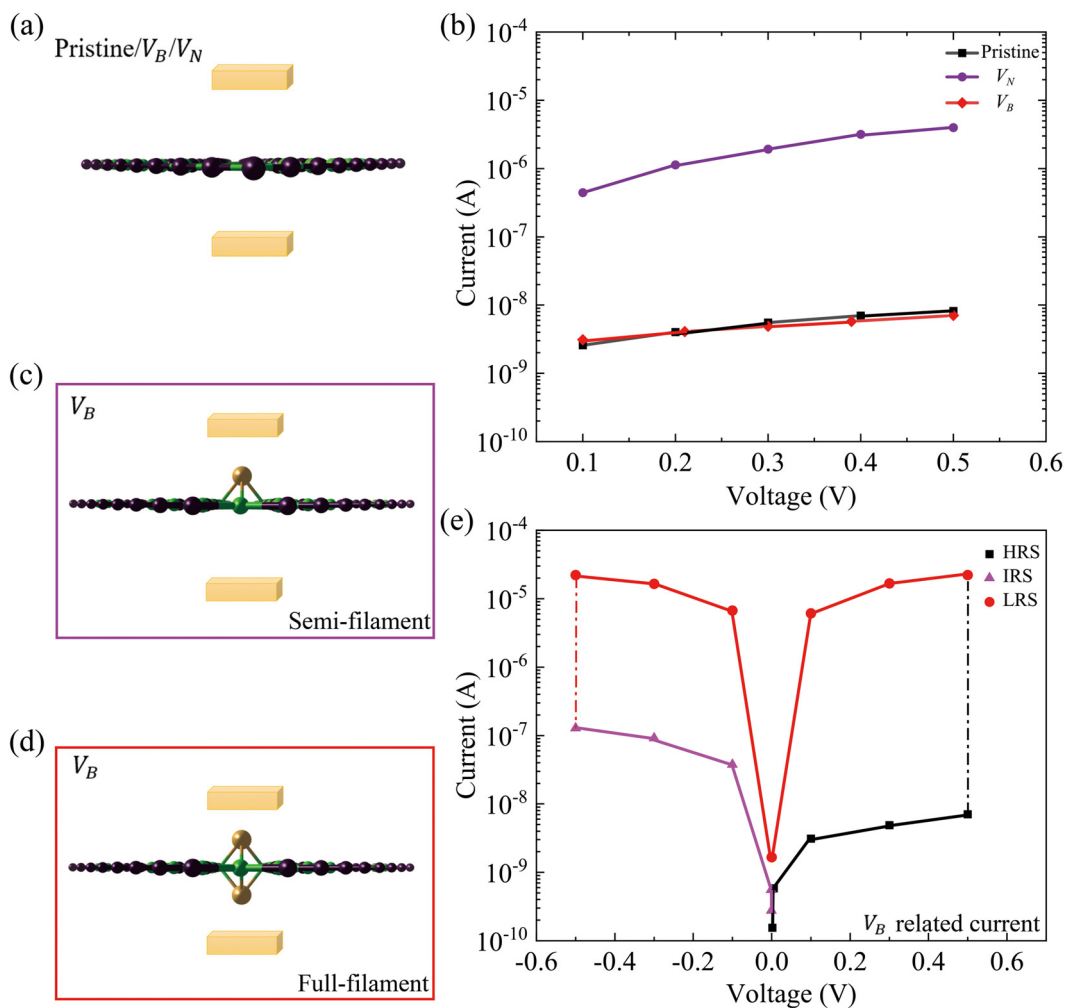
FIG. 2. (a) Schematic of pristine monolayer h-BN/monolayer h-BN with V_B/V_N used for calculating $I–V$ curves, and the yellow blocks schematically represent the electrodes. (b) $I–V$ curves of pristine monolayer h-BN and defective h-BN. (c) and (d) Schematics of memristors with a (c) semi-filament and (d) full-filament. (e) Calculated $I–V$ curves of resistive switching behavior in the memristor based on monolayer h-BN with V_B.

analyzed, and then we accordingly draw the schematics of energy barriers for electrons tunneling in the memristor based on a monolayer h-BN. As shown in Figs. 3(a)–3(c), the difference of DOS for three h-BN configurations (V_N, V_B, pristine) is mainly the E_F. The E_F of monolayer h-BN with V_N is significantly higher than those of other two cases due to the V_N defect state. This leads to a large reduction in the tunneling barrier Φ_2 and, thus, an enhancement of electrons tunneling in the V_N configuration, as seen in Figs. 3(d)–3(f). In contrast, the case of the V_B configuration is similar to that of the pristine sample and, thus, can maintain a good insulating OFF state, as shown in Fig. 2(b). Meanwhile, Φ_1 should be determined by the work function of metal.

Now, we try to figure out the possible conductive ON state. The absorption energy discussed above demonstrates Au atoms tend to bind with defects. Figure S3 shows that the Au atom inside the vdW gap is absorbed on V_B via chemical bonding with surrounding three

N atoms. Once this happens, it may expect that the tunneling barrier Φ_1 or Φ_2 will be largely canceled and may offer a practical way to form a conductive filament. Figure 2(c) exhibits the MIM structure with Au atoms adsorbed on the one side of V_B for the I–V calculation, see the simplified model in Fig. S1 for more details. Figure 2(e) shows the calculated I–V curve of this structure highlighted by purple-triangle data. As expected, the current signal has one order of magnitude raising compared to that without Au atom absorption at the same voltage, for example, 9.1×10^{-8} vs 4.9×10^{-9} A at $|0.3|$ V. However, it still cannot satisfy the experimentally observed 10^3 ON/OFF ratio.[31] One may naturally speculate that an extra Au atom can be adsorbed on the opposite site of V_B, and a full conductive atomic filament is formed, as shown in Fig. 2(d). Its I–V curve is also calculated as indicated by the red circles in Fig. 2(e). It can be clearly seen that when there is no filament, the device is initially at HRS, while a full conductive filament is formed, the device is set to an LRS. The current signal of this V_B pinning Au full
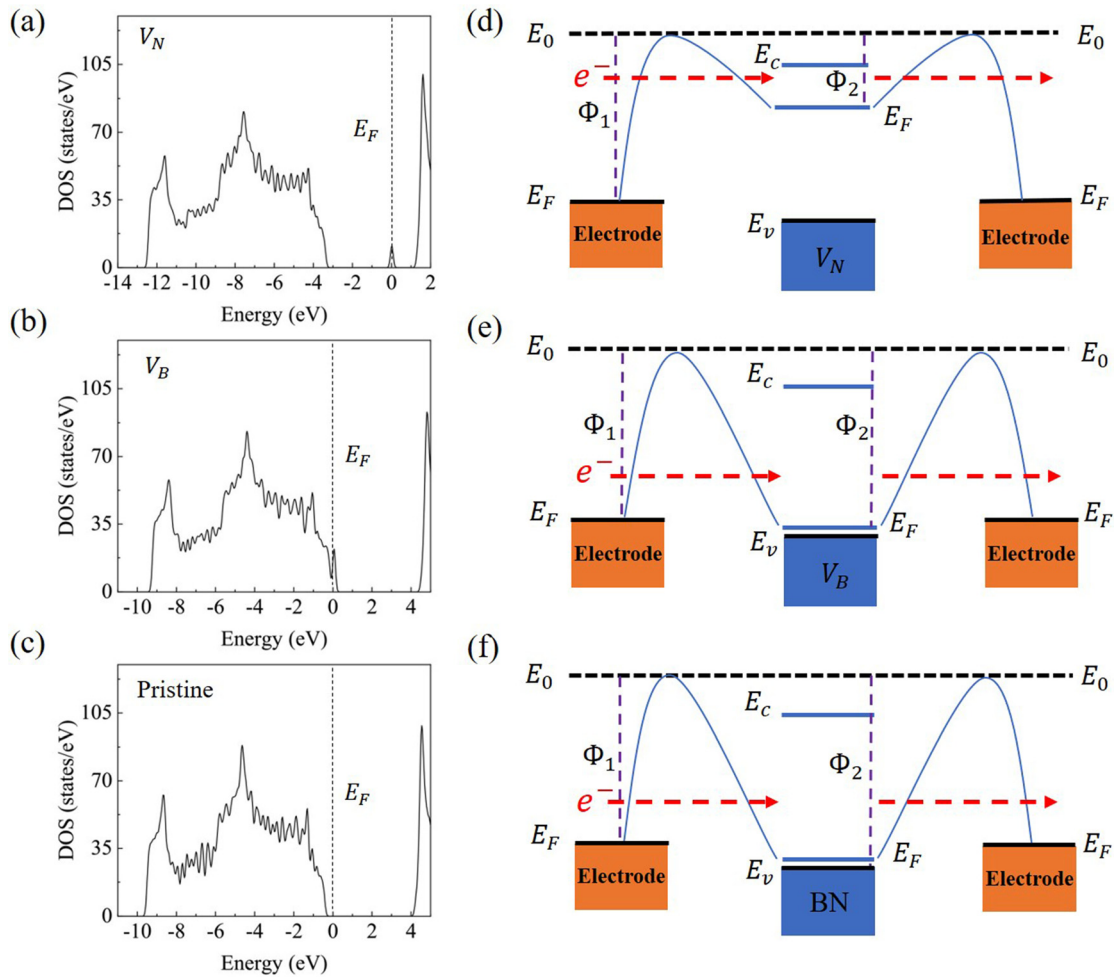
FIG. 3. (a)–(c) DOS for the monolayer h-BN with V_N, V_B, and without defects, respectively. (d)–(f) Schematics of energy barriers for electrons tunneling in memristors based on monolayer h-BN with V_N, V_B, and without defects, respectively. E_F represents the Fermi level. E_c indicates the conduction band minimum, and E_v indicates the valence band maximum. The orange and blue blocks schematically represent the energy bands occupied by electrons. Φ_1 and Φ_2 are the barrier heights for electrons tunneling between h-BN and Au electrodes.

conductive filament can reach up to three orders of magnitude higher than that without Au adsorption. In other words, they can act as the SET state and RESET state of this thinnest memristor. The relation between the current and defect density is also discussed in the supplementary material (Table S1). Note that, when the Au atom is partially absorbed on just one side of the monolayer h-BN, as seen in Fig. 2(c), it is an intermediate resistance state (IRS) with currents smaller than that of the LRS but higher than that of the HRS at the same voltage. The existence of partial adsorption may possibly explain the relatively large range of the resistances at HRS that was observed in previous reports.[31,35]

Though the proposal of the full atomic filament has provided a sufficient signal contrast for this thinnest memristor, how to form that is still not clear. Generally, metal atoms tend to migrate from one electrode to the opposite electrode along the direction of the applied electric field. Therefore, the possibility that Au atoms pass through the monolayer h-BN from one side to the other side should be taken into account. To figure out the possible migration processes, energy

barriers (E_b) for Au atoms passing through the h-BN monolayer in various situations were calculated. As seen in Fig. 4(a), the E_b for Au atoms penetrating the pristine sheet is 10.63 eV, which is too high to pass through. This result is a proof that the conductive channel cannot form in a pristine monolayer h-BN. With regard to the defective h-BN, the E_b for Au atoms to penetrate h-BN via V_B is only 0.832 eV [Fig. 4(b)], while the E_b for the case of V_N is 4.34 eV [Fig. 4(c)]. Here, the conductive filament is also not easy to form through V_N on account of the relatively high energy barrier. In contrast, the E_b for Au atoms penetrating the h-BN with V_{BN} is as low as 0.094 eV [Fig. 4(d)], which manifests that Au atoms could pass through the atomic sheet almost freely. The causation of such a low energy barrier is related to the large "room size" of the divacancy. The "room size" of different defects in monolayer h-BN is listed in Fig. S4 of the supplementary material, the approximate sizes of areas for V_{BN} are twice larger than that of V_B, and triply larger than that of V_N. Furthermore, the current of V_{BN} is two orders of magnitude higher than those of pristine h-BN and h-BN with V_B, see Table S2 in the supplementary material.
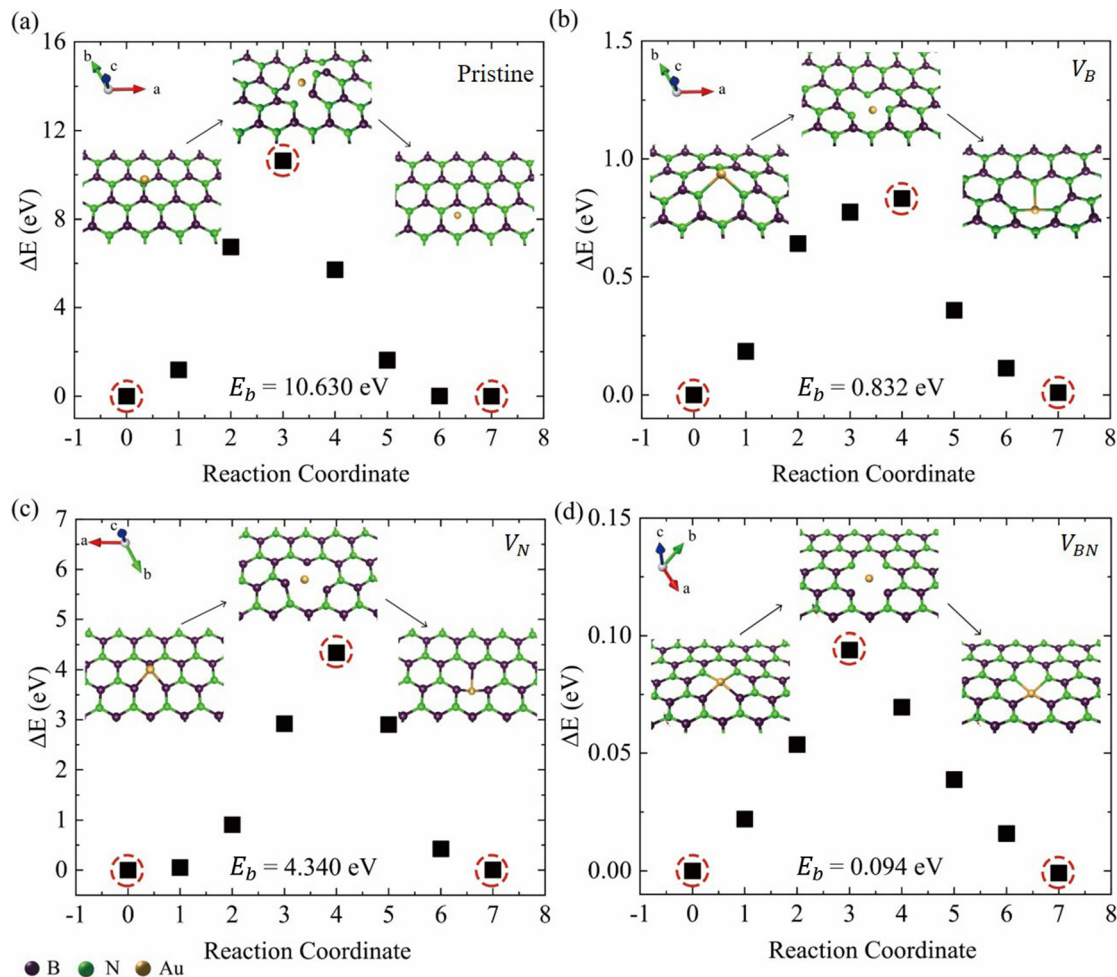
FIG. 4. The energy barrier for Au atoms passing through (a) pristine monolayer h-BN and monolayer h-BN with (b) V_B, (c) V_N, and (d) V_{BN}. The data marked by red circles indicate the initial, barrier, and final states. The corresponding structures are also exhibited in the insets.

(a)   (b)   (c)

300 K   500 K

● B   ● N   ● Au
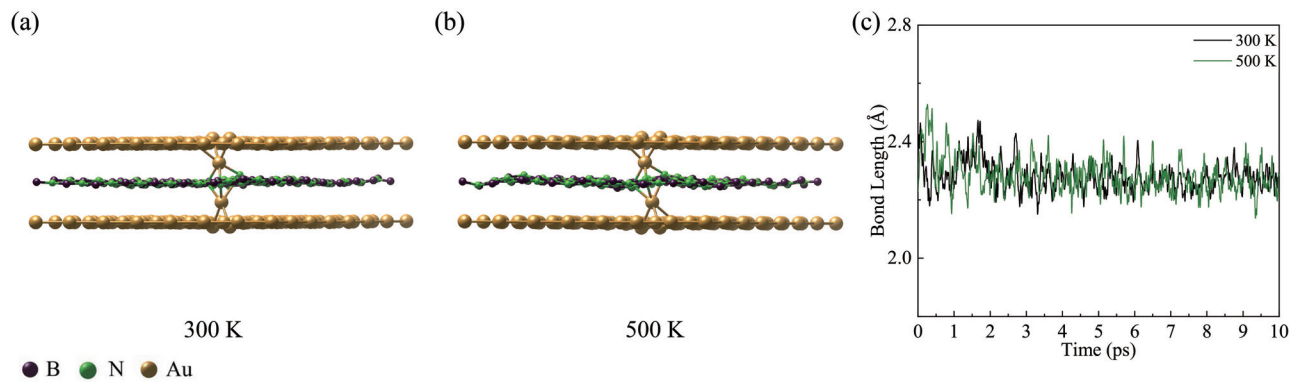
FIG. 5. Stability of the full conductive filament during 10-ps molecular dynamics (MD) simulations: the 10-ps moment snapshot at (a) 300 and (b) 500 K. (c) Evolution of the average Au-N bond length around V_B during the MDs. During the simulation, the Au (111) layers were fixed. In fact, even the Au (111) layers are removed, V_B itself can still hold the atomic filament without breaking at 500 K in 10-ps MD simulation.

To maintain a fine insulation without the short circuit in the atomically thin memristor, such large-size vacancies should be avoided. Considering that the formation energy of V_{BN} in monolayer h-BN is generally higher than that of monovacancy (see Table S3 in the supplementary material), V_{BN} is less likely to be produced. Therefore, the formation of full conductive filaments under an electric field in monolayer h-BN is most probably relying on V_B. The migration or penetration of Au atoms via V_B makes it possible to form the full conductive channel in this atomically thin memristor.

In order to verify whether the full conductive filament could exist stably in the thinnest memristor, 10-ps molecular dynamics (MD) simulations are further performed. The results manifest that the filament hold steadily at 300 K and even at 500 K, see the snapshots in Figs. 5(a) and 5(b). The evolution of the Au–N bond length also confirms that the Au atoms are stable in the V_B adsorption position, as seen in Fig. 5(c). Hence, the nonvolatility indeed could be maintained even at the thinnest limit of memristors.

Finally, considering both the bipolar and unipolar resistive switching behaviors have been experimentally observed in this thinnest memristor,[31,36] we deduce Joule-heating-effect induced atomic filament breaking is a possible reason for the conductive filament returning to a low conductive state.

In summary, the switching mechanism of the memristor based on a monolayer h-BN has been investigated by taking into account the atomic pictures and transport properties. It was found that the vdW gaps between Au electrodes and monolayer h-BN ensure the HRS of this thinnest memristor. The vacancy defects in monolayer h-BN provide active sites for Au-atom absorption, and thus, the conductive filament could be formed. Although the absorption of Au atoms on the one side of monolayer h-BN could introduce an increase in conductance, it can hardly provide sufficient signal contrast. When Au atoms penetrate the h-BN atomic sheet, a full conductive filament can be formed and fills up the vdW gaps. The calculated I–V characteristics of the memristor demonstrate that formation of full filaments can significantly enhance the conductance in the out-of-plane direction and, thus, provide sufficient ON/OFF ratios (10^3) to the insulation state. The conductive filament is only formed through V_B because the energy barrier for Au atoms to penetrate the atomic sheet with V_B is just 0.832 eV. Because defects in monolayer h-BN are possible to be controlled by defect engineering,[50,54] to maintain the insulation of the RRAM device at its 2D limit, V_N should be avoided. V_B also gives rise to the RESET state and IRS, which can appropriately explain the experimental phenomenon in previous works.[31,35] The thermal stability of the full conductive filament is also demonstrated at 500 K. This work proposes the key atomic picture of the resistive switching process in memristors at the 2D limit, which may help us develop the atomically thin devices for future high-density data storage and computation applications.

See the supplementary material for atomic structures, charge density difference, formation energies of the boron/nitrogen related defects, and the I-V characteristics of different h-BN supercells.

AUTHOR DECLARATIONS
Conflict of Interest

The authors have no conflicts to disclose.

Author Contributions

Xiao-Dong Li: Formal analysis (lead); Investigation (lead); Software (lead); Writing – original draft (lead). **Nian-Ke Chen:** Data curation (equal); Methodology (supporting); Supervision (lead); Writing – original draft (equal). **Bai-Qian Wang:** Formal analysis (supporting); Methodology (supporting). **Xian-Bin Li:** Conceptualization (lead); Funding acquisition (lead); Resources (lead); Writing – original draft (equal).

DATA AVAILABILITY

The data that support the findings of this study are available from the corresponding authors upon reasonable request.

REFERENCES

[1] G. M. Marega, Y. Zhao, A. Avsar, Z. Wang, M. Tripathi, A. Radenovic, and A. Kis, "Logic-in-memory based on an atomically thin semiconductor," Nature **587**, 72–77 (2020).

[2] D. Ielmini and H. S. P. Wong, "In-memory computing with resistive switching devices," Nat. Electron. **1**, 333–343 (2018).

[3] X. Xu, Y. Ding, S. X. Hu, M. Niemier, J. Cong, Y. Hu, and Y. Shi, "Scaling for edge inference of deep neural networks," Nat. Electron. **1**, 216–222 (2018).

[4] H. S. Stone, "A logic-in-memory computer," IEEE Trans. Comput. **c-19**, 73–78 (1970).

[5] W. H. Chen, C. Dou, K. X. Li, W. Y. Lin, P. Y. Li, J. H. Huang, J. H. Wang, W. C. Wei, C. X. Xue, Y. C. Chiu, Y. C. King, C. J. Lin, R. S. Liu, C. C. Hsieh, K. T. Tang, J. J. Yang, M. S. Ho, and M. F. Chang, "CMOS-integrated memristive non-volatile computing-in-memory for AI edge processors," Nat. Electron. **2**, 420–428 (2019).

[6] Y. Yang, M. Xu, S. Jia, B. Wang, L. Xu, X. Wang, H. Liu, Y. Liu, Y. Guo, L. Wang, S. Duan, K. Liu, M. Zhu, J. Pei, W. Duan, D. Liu, and H. Li, "A new opportunity for the emerging tellurium semiconductor: Making resistive switching devices," Nat. Commun. **12**, 6081 (2021).

[7] Y. Zhang, G. Q. Mao, X. Zhao, Y. Li, M. Zhang, Z. Wu, W. Wu, H. Sun, Y. Guo, L. Wang, X. Zhang, Q. Liu, H. Lv, K. H. Xue, G. Xu, X. Miao, S. Long, and M. Liu, "Evolution of the conductive filament system in HfO$_2$-based memristors observed by direct atomic-scale imaging," Nat. Commun. **12**, 7232 (2021).

[8] B. Govoreanu, G. S. Kar, Y. Chen, V. Paraschiv, S. Kubicek, A. Fantini, I. Radu, L. Goux, S. Clima, R. Degraeve, N. Jossart, O. Richard, T. Vandeweyer, K. Seo, P. Hendrickx, G. Pourtois, H. Bender, L. Altimime, D. J. Wouters, J. A. Kittl, and M. Jurczak, "10 × 10 nm^2 Hf/HfO$_x$ crossbar resistive RAM with excellent performance, reliability and low-energy operation," in *International Electron Devices Meeting* (IEEE, 2011).

[9] N. K. Chen, X. B. Li, J. Bang, X. P. Wang, D. Han, D. West, S. Zhang, and H. B. Sun, "Directional forces by momentumless excitation and order-to-order transition in Peierls-distorted solids: The case of GeTe," Phys. Rev. Lett. **120**, 185701 (2018).

[10] X. B. Li, X. Liu, X. Liu, D. Han, Z. Zhang, X. Han, H. B. Sun, and S. B. Zhang, "Role of electronic excitation in the amorphization of Ge-Sb-Te alloys," Phys. Rev. Lett. **107**, 015501 (2011).

[11] T. Tuma, A. Pantazi, M. L. Gallo, A. Sebastian, and E. Eleftheriou, "Stochastic phase-change neurons," Nat. Nanotechnol. **11**, 693–699 (2016).

[12] M. Salinga, B. Kersting, I. Ronneberger, V. P. Jonnalagadda, X. T. Vu, M. Le Gallo, I. Giannopoulos, O. Cojocaru-Mirédin, R. Mazzarello, and A. Sebastian, "Monatomic phase change memory," Nat. Mater. **17**, 681–685 (2018).

[13] Y. T. Huang, N. K. Chen, Z. Z. Li, X. B. Li, X. P. Wang, Q. D. Chen, H. B. Sun, and S. Zhang, "Mexican-hat potential energy surface in two-dimensional III$_2$-VI$_3$ materials and the importance of entropy barrier in ultrafast reversible ferroelectric phase change," Appl. Phys. Rev. **8**, 031413 (2021).

[14] S. Wang, L. Liu, L. Gan, H. Chen, X. Hou, Y. Ding, S. Ma, D. W. Zhang, and P. Zhou, "Two-dimensional ferroelectric channel transistors integrating ultra-fast memory and neural computing," Nat. Commun. **12**, 53 (2021).

[15] M. Mannini, F. Pineider, P. Sainctavit, C. Danieli, E. Otero, C. Sciancalepore, A. M. Talarico, M. A. Arrio, A. Cornia, D. Gatteschi, and R. Sessoli, "Magnetic memory of a single-molecule quantum magnet wired to a gold surface," Nat. Mater. **8**, 194–197 (2009).

[16] N. Magnani, C. Apostolidis, A. Morgenstern, E. Colineau, J. C. Griveau, H. Bolvin, O. Walter, and R. Caciuffo, "Magnetic memory effect in a transuranic mononuclear complex," Angew. Chem. **123**, 1734–1736 (2011).

[17] C. Liu, H. Chen, S. Wang, Q. Liu, Y. G. Jiang, D. W. Zhang, M. Liu, and P. Zhou, "Two-dimensional materials for next-generation computing technologies," Nat. Nanotechnol. **15**, 545–557 (2020).

[18] V. K. Sangwan and M. C. Hersam, "Neuromorphic nanoelectronic materials," Nat. Nanotechnol. **15**, 517–528 (2020).

[19] D. Wang, X. B. Li, D. Han, W. Q. Tian, and H. B. Sun, "Engineering two-dimensional electronics by semiconductor defects," Nano Today **16**, 30–45 (2017).

[20] S. Y. Xie, Y. Wang, and X. B. Li, "Flat boron: A new cousin of graphene," Adv. Mater. **31**, 1900392 (2019).

[21] H. Tian, Q. Guo, Y. Xie, H. Zhao, C. Li, J. J. Cha, F. Xia, and H. Wang, "Anisotropic black phosphorus synaptic device for neuromorphic applications," Adv. Mater. **28**, 4991–4997 (2016).

[22] M. Wang, S. Cai, C. Pan, C. Wang, X. Lian, Y. Zhuo, K. Xu, T. Cao, X. Pan, and B. Wang, "Robust memristors based on layered two-dimensional materials," Nat. Electron. **1**, 130–136 (2018).

[23] X. Zhu, D. Li, X. Liang, and W. D. Lu, "Ionic modulation and ionic coupling effects in MoS$_2$ devices for neuromorphic computing," Nat. Mater. **18**, 141–148 (2019).

[24] Q. A. Vu, H. Kim, V. L. Nguyen, U. Y. Won, S. Adhikari, K. Kim, Y. H. Lee, and W. J. Yu, "A high-on/off-ratio floating-gate memristor array on a flexible substrate via CVD-grown large-area 2D layer stacking," Adv. Mater. **29**, 1703363 (2017).

[25] L. Wang, W. Liao, S. L. Wong, Z. G. Yu, S. Li, Y. F. Lim, X. Feng, W. C. Tan, X. Huang, L. Chen, L. Liu, J. Chen, X. Gong, C. Zhu, X. Liu, Y. W. Zhang, D. Chi, and K. W. Ang, "Artificial synapses based on multiterminal memtransistors for neuromorphic application," Adv. Funct. Mater. **29**, 1901106 (2019).

[26] R. Xu, H. Jang, M. H. Lee, D. Amanov, Y. Cho, H. Kim, S. Park, H. J. Shin, and D. Ham, "Vertical MoS$_2$ double-layer memristor with electrochemical metallization as an atomic-scale synapse with switching thresholds approaching 100 mV," Nano Lett. **19**, 2411–2417 (2019).

[27] C. Pan, Y. Ji, N. Xiao, F. Hui, K. Tang, Y. Guo, X. Xie, F. M. Puglisi, L. Larcher, E. Miranda, L. Jiang, Y. Shi, I. Valov, P. C. McIntyre, R. Waster, and M. Lanza, "Coexistence of grain-boundaries-assisted bipolar and threshold resistive switching in multilayer hexagonal boron nitride," Adv. Funct. Mater. **27**, 1604811 (2017).

[28] H. Zhao, Z. Dong, H. Tian, D. DiMarzi, M. G. Han, L. Zhang, X. Yan, F. Liu, L. Shen, S. J. Han, S. Cronin, W. Wu, J. Tice, J. Guo, and H. Wang, "Atomically thin femtojoule memristive device," Adv. Mater. **29**, 1703232 (2017).

[29] Y. Shi, X. Liang, B. Yuan, V. Chen, H. Li, F. Hui, Z. Yu, F. Yuan, E. Pop, H. S. P. Wong, and M. Lanza, "Electronic synapses made of layered two-dimensional materials," Nat. Electron. **1**, 458–465 (2018).

[30] K. Zhu, X. Liang, B. Yuan, M. A. Villena, C. Wen, T. Wang, S. Chen, F. Hui, Y. Shi, and M. Lanza, "Graphene–boron nitride–graphene cross-point memristors with three stable resistive states," ACS Appl. Mater. Interfaces **11**, 37999–38005 (2019).

[31] X. Wu, R. Ge, P. A. Chen, H. Chou, Z. Zhang, Y. Zhang, S. Banerjee, M. H. Chiang, J. C. Lee, and D. Akinwande, "Thinnest nonvolatile memory based on monolayer h-BN," Adv. Mater. **31**, 1806790 (2019).

[32] R. Ge, X. Wu, M. Kim, J. Shi, S. Sonde, L. Tao, Y. Zhang, J. C. Lee, and D. Akinwande, "Atomristor: Nonvolatile resistance switching in atomic sheets of transition metal dichalcogenides," Nano Lett. **18**, 434–441 (2018).

[33] M. Kim, R. Ge, X. Wu, X. Lan, J. Tice, J. C. Lee, and D. Akinwande, "Zero-static power radio-frequency switches based on MoS$_2$ atomristors," Nat. Commun. **9**, 2524 (2018).

[34] M. Kim, E. Pallecchi, R. Ge, X. Wu, G. Ducournau, J. C. Lee, H. Happy, and D. Akinwande, "Analogue switches made from boron nitride monolayers for application in 5G and terahertz communication systems," Nat. Electron. **3**, 479–485 (2020).

[35] R. Ge, X. Wu, L. Liang, S. M. Hus, Y. Gu, E. Okogbue, H. Chou, J. Shi, Y. Zhang, S. K. Banerjee, Y. Jung, J. C. Lee, and D. Akinwande, "A library of atomically thin 2D materials featuring the conductive-point resistive switching phenomenon," Adv. Mater. **33**, 2007792 (2021).

[36] R. D. Nikam, K. G. Rajput, and H. Hwang, "Single-atom quantum-point contact switch using atomically thin hexagonal boron nitride," Small **17**, 2006760 (2021).

[37] Y. Li, L. Loh, S. Li, L. Chen, B. Li, M. Bosman, and K. W. Ang, "Anomalous resistive switching in memristors based on two-dimensional palladium diselenide using heterophase grain boundaries," Nat. Electron. **4**, 348–356 (2021).

[38] S. M. Hus, R. Ge, P. A. Chen, L. Liang, G. E. Donnelly, W. Ko, F. Huang, M. H. Chiang, A. P. Li, and D. Akinwande, "Observation of single-defect memristor in an MoS$_2$ atomic sheet," Nat. Nanotechnol. **16**, 58–62 (2021).

[39] P. Hohenberg and W. Kohn, "Inhomogeneous electron gas," Phys. Rev. **136**, B864 (1964).

[40] W. Kohn and L. J. Sham, "Density function theory," Phys. Rev. **140**, A1133–A1138 (1965).

[41] A. P. Jauho, N. S. Wingreen, and Y. Meir, "Time-dependent transport in interacting and noninteracting resonant-tunneling systems," Phys. Rev. B **50**, 5528 (1994).

[42] G. Kresse and J. Furthmüller, "Efficiency of *ab-initio* total energy calculations for metals and semiconductors using a plane-wave basis set," Comput. Mater. Sci. **6**, 15–50 (1996).

[43] G. Henkelman, B. P. Uberuaga, and H. Jónsson, "A climbing image nudged elastic band method for finding saddle points and minimum energy paths," J. Chem. Phys. **113**, 9901–9904 (2000).

[44] J. P. Perdew, K. Burke, and M. Ernzerhof, "Generalized gradient approximation made simple," Phys. Rev. Lett. **77**, 3865 (1996).

[45] J. Taylor, H. Guo, and J. Wang, "*Ab initio* modeling of quantum transport properties of molecular electronic devices," Phys. Rev. B **63**, 245407 (2001).

[46] J. M. Soler, E. Artacho, J. D. Gale, A. García, J. Junquera, P. Ordejón, and D. Sánchez-Portal, "The SIESTA method for *ab initio* order-N materials simulation," J. Phys.: Condens. Matter **14**, 2745 (2002).

[47] N. Troullier and J. L. Martins, "Efficient pseudopotentials for plane-wave calculations," Phys. Rev. B **43**, 1993 (1991).

[48] M. Gao, A. Lyalin, and T. Taketsugu, "Catalytic activity of Au and Au_2 on the h-BN surface: Adsorption and activation of O_2," J. Phys. Chem. C **116**, 9054–9062 (2012).

[49] B. Huang and H. Lee, "Defect and impurity properties of hexagonal boron nitride: A first principles calculation," Phys. Rev. B **86**, 245406 (2012).

[50] K. K. Kim, A. Hsu, X. Jia, S. M. Kim, Y. Shi, M. Hofmann, D. Nezich, J. F. Rodriguez-Nieva, M. Dresselhaus, T. Palacios, and J. Kong, "Synthesis of monolayer hexagonal boron nitride on Cu foil using chemical vapor deposition," Nano Lett. **12**, 161–166 (2012).

[51] Z. Hu, Z. Wu, C. Han, J. He, Z. Ni, and W. Chen, "Two-dimensional transition metal dichalcogenides: Interface and defect engineering," Chem. Soc. Rev. **47**, 3100–3128 (2018).

[52] U. Chandni, K. Watanabe, T. Taniguchi, and J. Eisenstein, "Evidence for defect-mediated tunneling in hexagonal boron nitride-based junctions," Nano Lett. **15**, 7329–7333 (2015).

[53] G. H. Lee, Y. J. Yu, C. Lee, C. Dean, K. L. Shepard, P. Kim, and J. Hone, "Electron tunneling through atomically flat and ultrathin hexagonal boron nitride," Appl. Phys. Lett. **99**, 243114 (2011).

[54] J. C. Koepke, J. D. Wood, Y. Chen, S. W. Schmucker, X. Liu, N. N. Chang, L. Nienhaus, J. W. Do, E. A. Carrion, J. Hewaparakrama, A. Rangarajan, I. Datye, R. Mehta, R. T. Haasch, M. Gruebele, G. S. Girolami, E. Pop, and J. W. Lyding, "Role of pressure in the growth of hexagonal boron nitride thin films from ammonia-borane," Chem. Mater. **28**, 4169–4179 (2016).